Equivalent circuits in nanopore-based electrochemical systems

Patricio Ramirez,[a,*] Javier Cervera,[b,**] Vladimir García-Morales,[b] Saima Nasir,[c,d] Mubarak Ali,[c,d] Wolfgang Ensinger,[d] Salvador Mafe[b]

[a]*Departament de Física Aplicada, Universitat Politècnica de València, E-46022 València (Spain)*
[b]*Departament de Física de la Terra i Termodinàmica, Universitat de València, E-46100 Burjassot (Spain)*
[c]*Materials Research Department, GSI Helmholtzzentrum für Schwerionenforschung, D-64291 Darmstadt, Germany*
[d]*Department of Material- and Geo-Sciences, Technische Universität Darmstadt, D-64287 Darmstadt (Germany)*

Single-nanopore membranes constitute physical models for biological ion channels and are also central to electrochemical energy transducers, logical circuits in sensors and actuators, and converters in bioelectrical interfaces. The membrane potential, defined as the electrical potential difference established between two different ionic solutions separated by the membrane, is crucial for the electrical coupling of nanofluidic concentration cells to electronic components such as load capacitors and resistors. Here we analyze, theoretically and experimentally, the validity of basic principles governing electric circuit theory such as the Thévenin equivalent circuit, the additivity of voltages and resistances, and the Millman theorem in nanopore-based concentration cells. To this end, we consider a wide range of practical conditions with respect to salt concentrations, nanopore asymmetry, electrical capacitances, and series and parallel arrangements. Additionally, we investigate the scaling of the single pore results to the multipore case. The results obtained suggest that basic circuit models offer approximate tools to guide the analysis of the nanofluidic concentration cells.

*patraho@fis.upv.es, **jcervera@uv.es

Keywords: Conical nanopore, membrane potential, equivalent circuits, nanofluidics, concentration cells

1. Introduction

Single-nanopore membranes provide biomimetic models for the protein ion channels inserted in cell membranes and are central to bioinspired nanofluidic iontronics mimicking brain-like functionalities [1–3]. These nanoscale pores also act as basic units of nanofluidic concentration cells in electrochemical energy transducers, enable logical circuits in sensors and actuators, and facilitate signal processing in bioelectrical interfaces [4–10]. The membrane potential, defined as the electrical potential difference established between two different ionic solutions separated by the membrane, is the most significant electrical magnitude in biological membranes and nanopore-based electrochemical devices [2,11,12] because it regulates the fluxes of matter, energy, and information. Therefore, the electrical properties of membrane potentials in nanofluidic concentration cells consisting of two half-cells, each of which containing the same electrodes but different salt concentrations, are of wide interest in applied science and technology.

We do not address here the problem of osmotic energy harvesting in membranes and nanopores, whose characteristics and efficiency has been studied in great detail previously [13–17]. Rather, we will focus on the validity of basic equivalent circuits as useful tools to characterize nanopore-based electrochemical cells. Note that the electrical coupling of nanopore ionic conduction to electronic components such as load capacitors and resistors is crucial for an efficient functionality of the resulting hybrid circuits [3,4,18]. Also, multipore membranes and circuits with multiple nanopores are used in practical applications [6,8,17,19]. We will consider basic principles such as the Thévenin equivalent circuit, the voltages and resistances additivity, and the Millman theorem under a wide range of salt concentrations and electrical capacitances, including series and parallel arrangements.

2. Experimental methods

Figs. 1a and b show the electrochemical cell enclosed in a double-layer magnetic shield (Amuneal Manufacturing, Philadelphia, PA) and placed on an anti-vibration table (Technical Manufacturing Corporation, Peabody, Massachusetts). The single-pore membranes consisted of a 12.5-µm thick polyimide (PI) foil (Kapton50 HN, DuPont) irradiated at the *UNILAC* linear accelerator (GSI, Darmstadt) with swift heavy Au ions of energy 11.4 MeV per nucleon [20,21]. The ion tracks were converted into conical nanopores following asymmetric track-etching procedures [20–22]. These procedures led to carboxylate residues of effective surface charge densities in the range –0.1 - (–1.0) e/nm^2, where e is the elementary charge, at neutral pH values [18]. Pore radii were estimated to be in the ranges 10 – 40 nm for the cone tip and 300 – 800 nm for the cone base from SEM images of pore fractures and electrical conductance measurements [18]. Input potentials and output currents were measured using Ag|AgCl electrodes with 2M KCl solution salt bridges in the left (L, pore tip) and right (R, pore base) solutions (Fig. 2). Approximately neutral pH solution values were found before and after each measurement; the ambient temperature T was kept at 295 K.

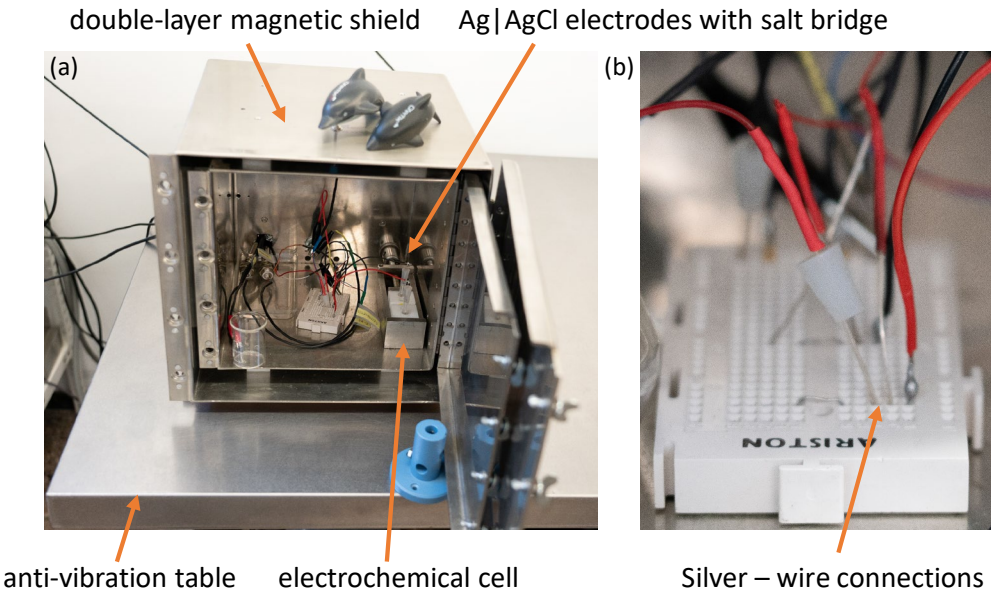

Fig. 1 (a) Photograph of the experimental setup with the electrochemical cell placed within a magnetic shield and mounted on an anti-vibration table. (b) Detail of the silver wire connections required to avoid noise effects.

The steady-state current (I)–voltage (V) curves were measured using different electrical arrangements consisting of a Keithley 6514 high input impedance electrometer, and a Keithley 6487 pico-ammeter/voltage source (Keithley Instruments, Cleveland, Ohio). The asymmetric nanopore (Fig. 2a) exhibited low electrical conductances when the current entered the cone base ($V < 0$) and high conductances when it entered the cone tip ($V > 0$) [18,23]. Each measurement was repeated several times with good data reproducibility, as shown previously [18,12]. Figs. 2a–d show how the Thévenin voltage (V_{Th}), the Norton short-circuit current (I_N), and the Thévenin resistance (R_{Th}) can be accurately determined by three independent experiments. In order to achieve high reproducibility and to reduce noise effects, Ag wires were used to connect the various circuit elements placed inside the double-layer magnetic shield and mounted on the anti-vibration table of Fig. 1.

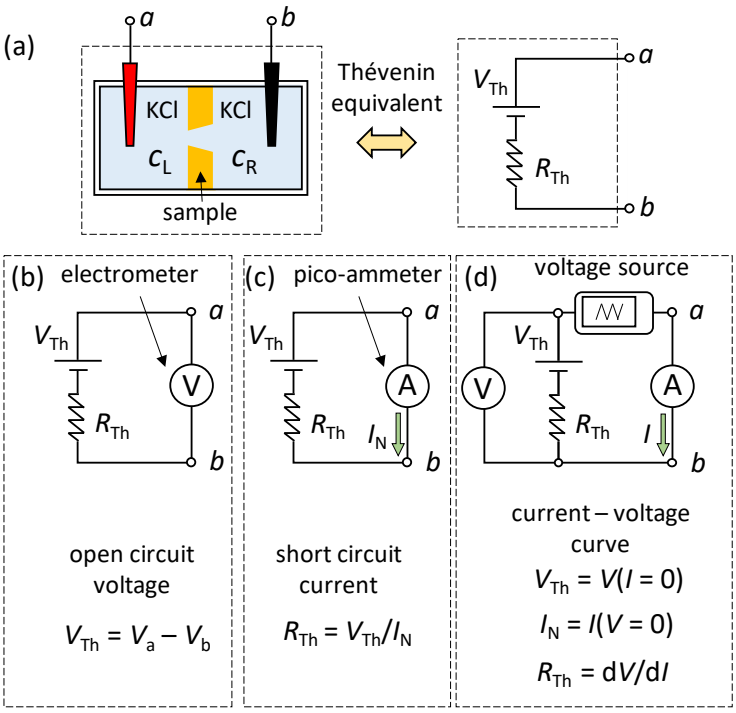

Fig. 2 (a) Thévenin equivalent of the nanofluidic cell with concentrations c_L and c_R. The Thévenin voltage (V_{Th}) and resistance (R_{Th}), and the Norton short-circuit current (I_N) are measured from three independent experiments. (b) The voltage V_{Th} was measured using a high input impedance electrometer as the potential difference between points *a* and *b* under open circuit conditions. (c) The short circuit Norton current (I_N) was measured using a pico-ammeter under closed circuit conditions, and the resistance R_{Th} was obtained from $R_{Th} = dV/dI$ in the steady V–I curve (d) The variable voltage source produced a low-frequency triangular wave that, together with the electrometer and the ammeter, allowed the measurement of the nanopore $V-I$ curve. The values of V_{Th} and I_N could be obtained from the intercepts points of this curve at the V-axis (ordinate) and I-axis (abscissa), respectively. For the check of consistency, the resistance R_{Th} was then calculated from the slope of the approximately linear $V-I$ curve.

3. Results and discussion

Fig. 3a shows the Thévenin equivalent circuits corresponding to the two conical pore positions relative to the imposed concentration difference. Note the stability of the measured

Thévenin voltage (Fig. 3b) and Norton current (Fig. 3c) as well as the numerical agreement of these values with those obtained from the *V*–*I* curve at low voltage amplitudes (Fig. 3d). As expected, V_{Th} and I_N take relatively high values when the dilute solution faces the cone tip (position 1) rather than when it faces the cone base (position 2) [17]: the Debye screening of the pore charges is lower, and thus the ionic selectivity is higher, in the first case than in the second case [18]. The results obtained with the three experimental methods of Figs. 3b–d strongly suggest that basic principles of traditional electric circuit theory can still be applied for the physical characterization of nanofluidic cells with ionic currents in the range 0.01 – 0.1 nA.

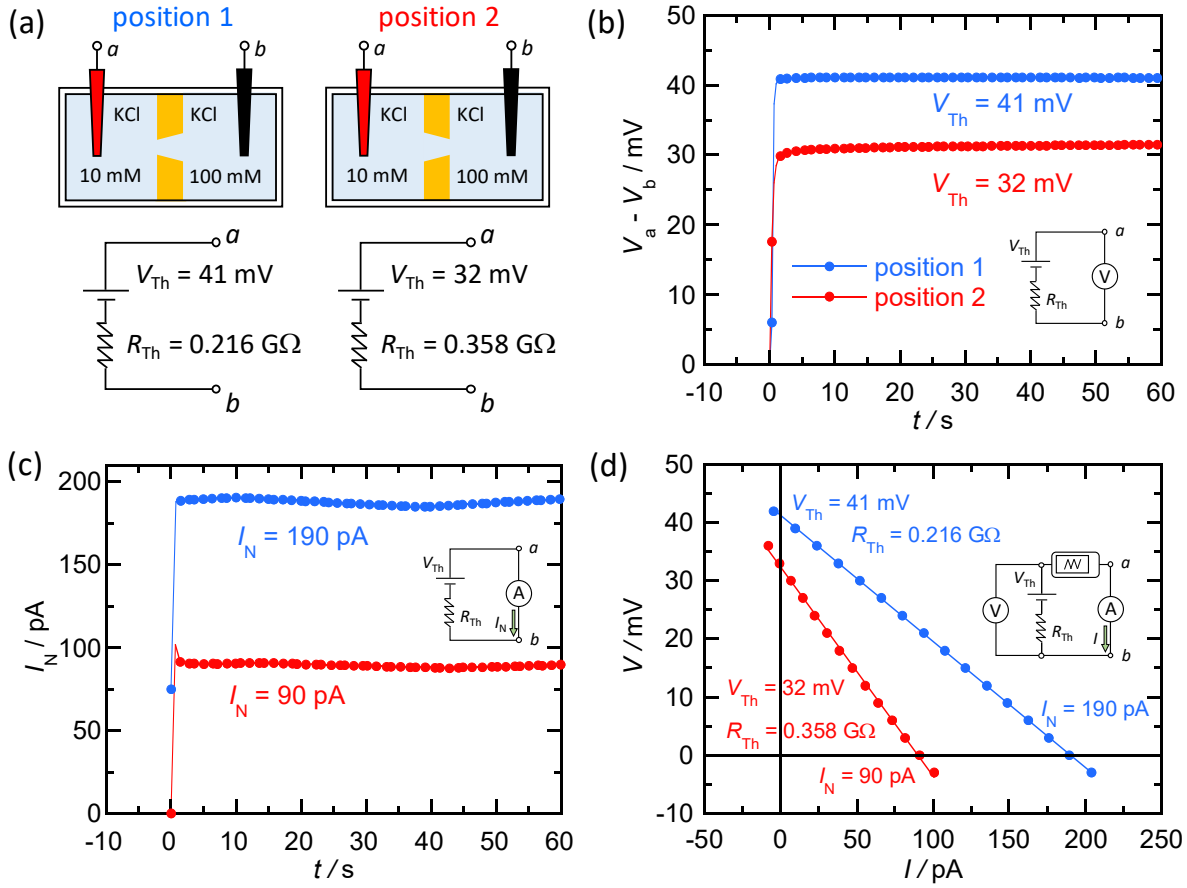

Fig. 3 (a) The Thévenin equivalent circuits of two conical pore positions for nanopore *sample # 1* with the concentrations c_L = 10 mM and c_R = 100 mM KCl. (b) The steady-state value of the time (*t*) dependent potential difference between points *a* and *b* under open circuit conditions gives V_{Th}. (c) The steady-state current between points *a* and *b* under short circuit conditions

gives I_N. (d) The nanopore V–I curve gives R_{Th} from Ohm's law. Note that the intercepts points of this curve at the ordinate and abscissa axes give consistent values of V_{Th} and I_N.

Figs. 4a–d show the effect of the concentration difference on the electrical parameters that characterize the nanofluidic cell. Together with the values of V_{Th}, I_N, and R_{Th} (Figs. 4a–c) defined in Fig. 2, the cell power $P_{max} = V_{Th}^2/(4R_{Th})$ obtained from the maximum power transfer theorem is also shown (Fig. 4d). In each case, the continuum lines are calculated using a Poisson-Nernst-Planck model [24,25] with the nanopore radii a_{tip} = 8 nm and a_{base} = 250 nm, thickness d = 12 μm, shape factor d/h = 25, and surface charge density σ = –0.7 e/nm^2. As in Fig. 3, the nanopore position 2 gives values of V_{Th}, I_N, and P_{max} lower than those of position 1; note the logarithmic scale of Figs. 4b–d. Additional data obtained with other monovalent (LiCl, NaCl, and CsCl) and divalent ($BaCl_2$, $MgCl_2$, and $CaCl_2$) cation salts confirmed further the general validity of the experimental methods used.

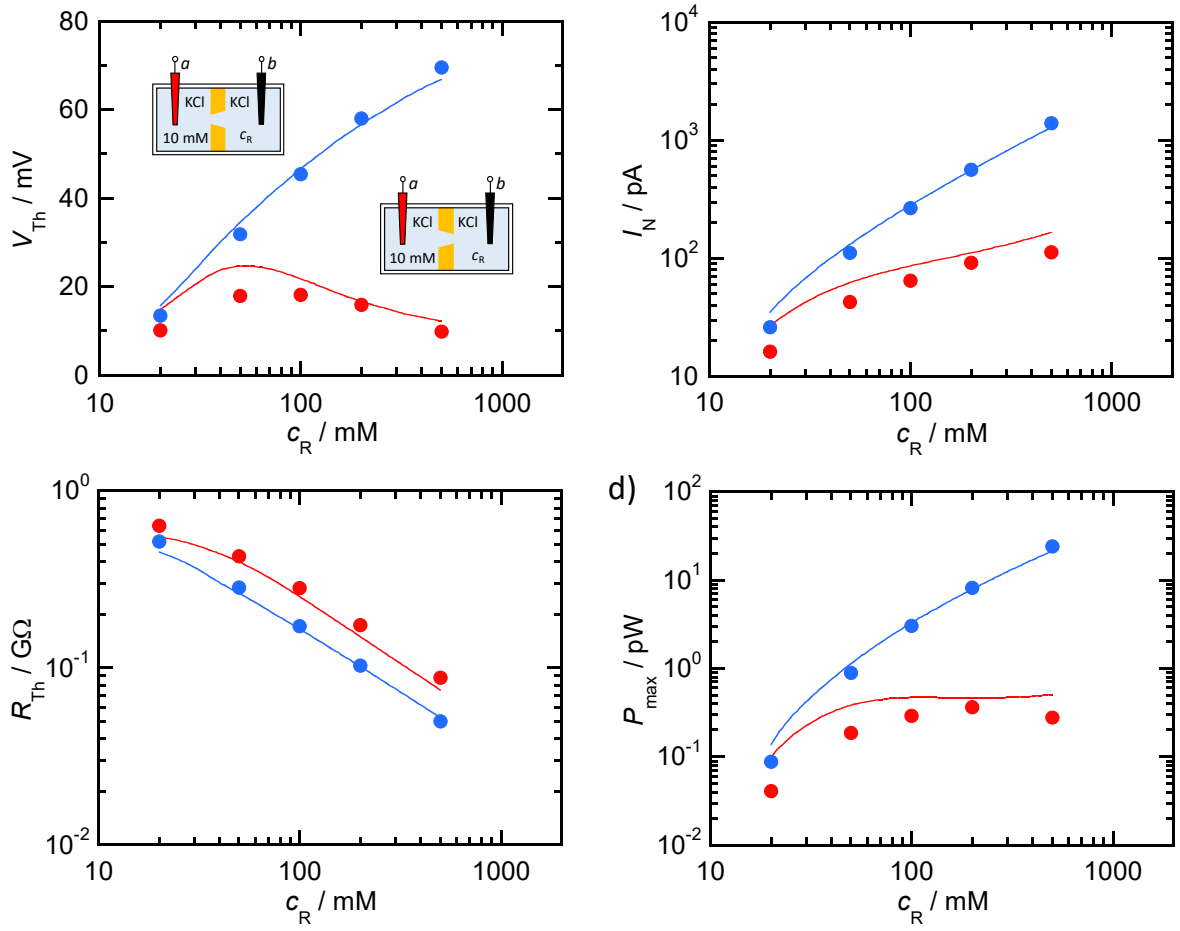

Fig. 4 (a) The voltage V_{Th} as a function of the concentration c_R for nanopore *sample # 2*. (b) The current I_N as a function of the concentration c_R. (c) The resistance R_{Th} as a function of the concentration c_R. (d) The maximum cell power $P_{max} = V_{Th}^2/4R_{Th}$ as a function of the concentration c_R. In all cases, c_L = 10 Mm KCl and the continuum lines are obtained with a Poisson-Nernst-Planck model previously proposed [24].

Figs. 5a–d consider behavior of the nanofluidic cell with a load capacitor. The measured electric circuit parameters are listed in Table 1. As expected, the steady-state capacitor voltage attained at long times (Fig. 5a) is approximately equal to the Thévenin voltage (Fig. 3b). Note also the close correspondence observed between the charging voltage and the current curves (Figs. 5a and 5b). The effect of the capacitance on the charging curves (Fig. 5c) shows that the capacitor voltage takes the same steady-state value (the Thévenin voltage) in all cases. The

continuum lines correspond to the equivalent circuit theoretical curves. Fig. 5d considers the effect of the cell concentration difference on the capacitor charging curve. Prior to the measurements and for the sake of consistency, the cell electrical parameters were obtained for each KCl concentration difference employed in nanopore position 1, as shown in Table 1. Remarkably, the nanofluidic cell behaves in a predictable and reliable way all over the capacitance and concentration ranges studied.

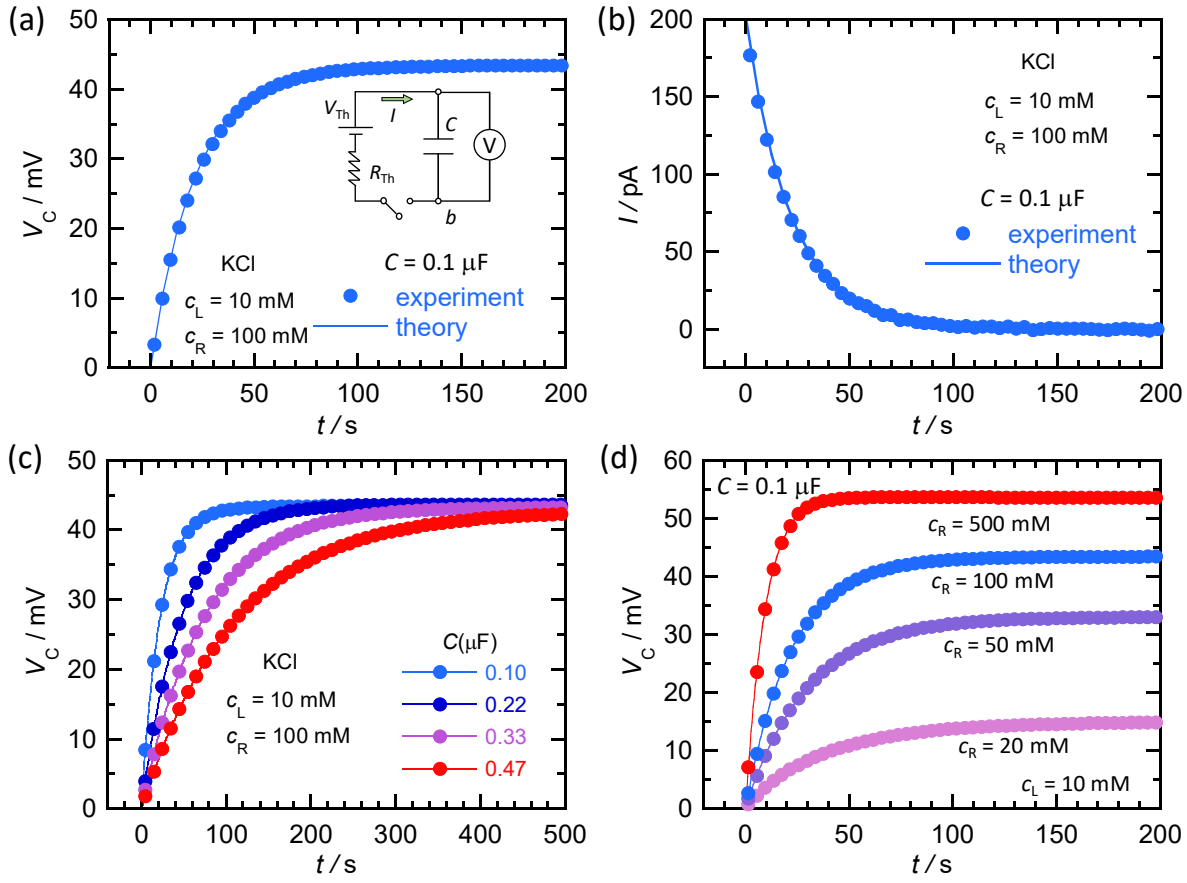

Fig. 5 (a) Charging capacitor curve for nanopore *sample # 1* and position 1. The capacitor voltage V_C measured with the electrometer is shown as a function of time for the capacitance C and salt concentration values in the *inset*. The continuum line corresponds to the theoretical charging curve $V_C = V_{Th}[1–\exp(–t/R_{Th}C)]$. (b) The circuit current I can be obtained from the experimental data as $I = C(\mathrm{d}V_C/\mathrm{d}t)$. The continuum line corresponds to the theoretical current curve $I = I_N\exp(–t/R_{Th}C)$. (c) The charging curves parametric in the capacitance C for nanopore

position 1. The continuum lines correspond to the above theoretical equation. (d) The charging curves parametric in the concentration c_R for c_L = 10 Mm, C = 0.1 μF, and nanopore position 1. The continuum lines correspond to the theoretical curves obtained using the previously measured electrical characteristics of Table 1.

c_R / mM	V_{Th} / mV	R_{Th} / GΩ	I_N / pA
20	15.1	0.458	33
50	33.1	0.304	109
100	43.6	0.216	193
500	54.7	0.095	571

Table 1. Nanoflidic concentration cell characteristics obtained following the experimental methods of Fig. 2 for the case of *sample #1*, nanopore position 1, and c_L = 10 mM KCl.

Figs. 6a–d analyze the nanofluidic cell behavior with a load resistor. Note that the equivalent circuit characteristics (Fig. 6a) obtained in this new experimental run using the experimental methods of Fig. 2 differ from those of Fig. 3a. These changes should be ascribed to the nanopore state modification after many experimental runs (Figs. 3–6). Despite this fact, we must emphasize that the voltage drops at the load resistor do not change with time during each experiment and show a good reproducibility between independent measurements (Figs. 6b and 6c) also in this case. Moreover, the results are in good agreement with the voltage divider model (Fig. 6c) and the dissipated power shows a maximum value at the Thévenin resistance, as predicted by the maximum power transfer theorem (Fig. 6d). These experimental facts confirm further the validity of equivalent circuit methods for analyzing nanofluidic concentration cells with dissipated powers of the order of 1 pW (Fig. 6d).

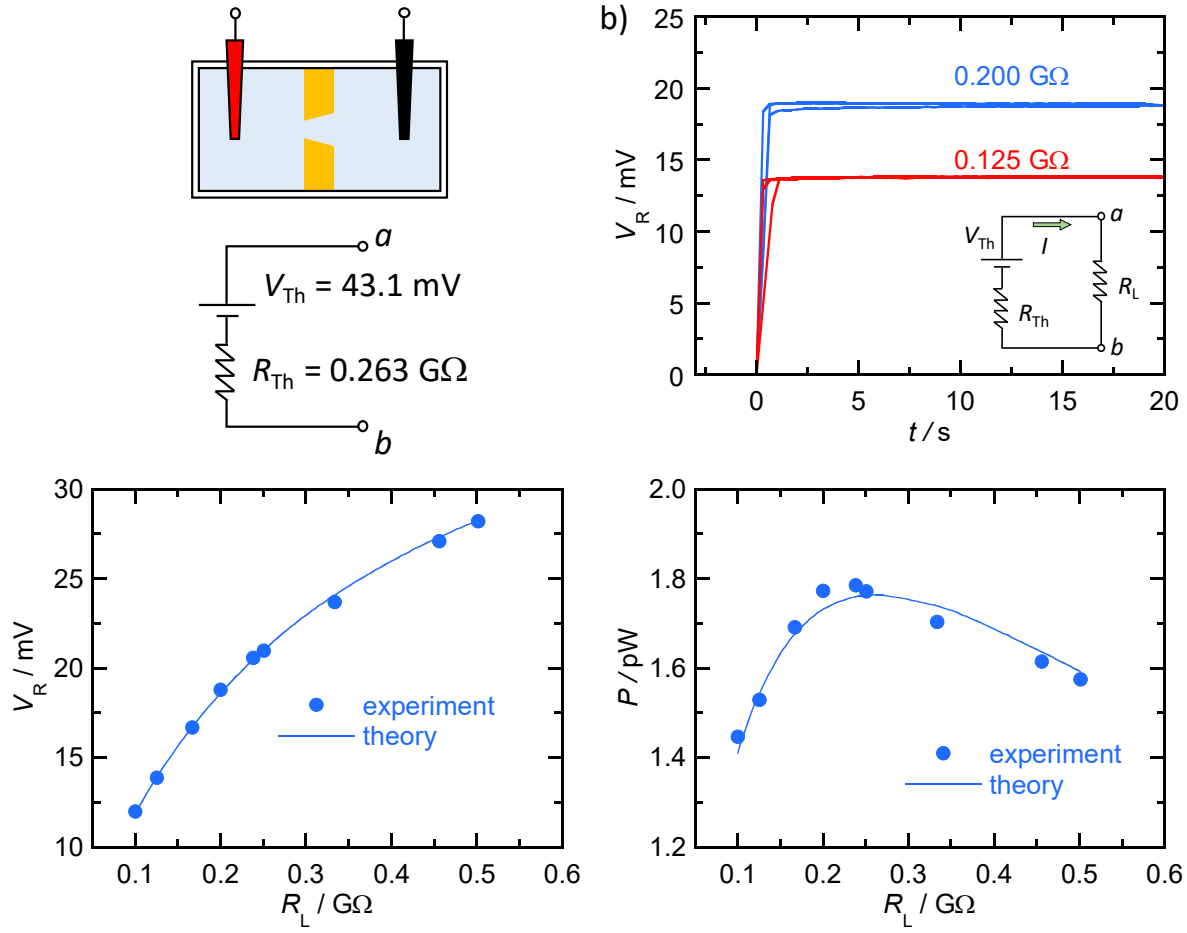

Fig. 6 (a) The Thévenin equivalent circuit obtained for *sample #1* and position 1 for this new experimental run using the methods of Fig. 2, with c_L = 10 mM and c_R = 100 mM KCl. (b) The voltage drop V_R at the load resistor R_L, measured with the high input impedance electrometer (*inset*), as a function of time. Note that three independent measurements were conducted for the two load resistors used. Also, fresh salt solutions were used for each measurement to avoid any leakage from the electrode salt bridges. (c) The voltage drop V_R as a function of the load resistance R_L. Each experimental point is the average value of three independent measurements, as shown in Fig. 6b. The continuum line corresponds to the theoretical results obtained using a voltage divider model giving $V_R = [R_L/(R_L + R_{Th})]V_{Th}$, with the cell parameters of Fig. 6a. (d) Power dissipated in the load resistance as a function of R_L. The maximum power is obtained at $R_L = R_{Th}$, in agreement with the equation for the maximum power transfer (continuous line).

Figs. 7a–d consider the cases of series and parallel cell arrangements for the nanopore samples *#1* and *#3* (Fig. 7a). The equivalent circuit parameters of Figs. 7b–d are given in Table 2. The additivity of the respective Thévenin voltages and resistances together with the validity of Millman's theorem for the maximum power transfer, obtained with the electrical characteristics of Figs. 7a and 7b, are confirmed in Table 2. Note the different time constants and steady-state values corresponding to the distinct electrical configurations observed in the charging curves of Fig. 7d. Again, these result suggest that the equivalent circuit models characteristic of applied physics are also useful for characterizing of nanofluidic concentration cells and their series and parallel associations.

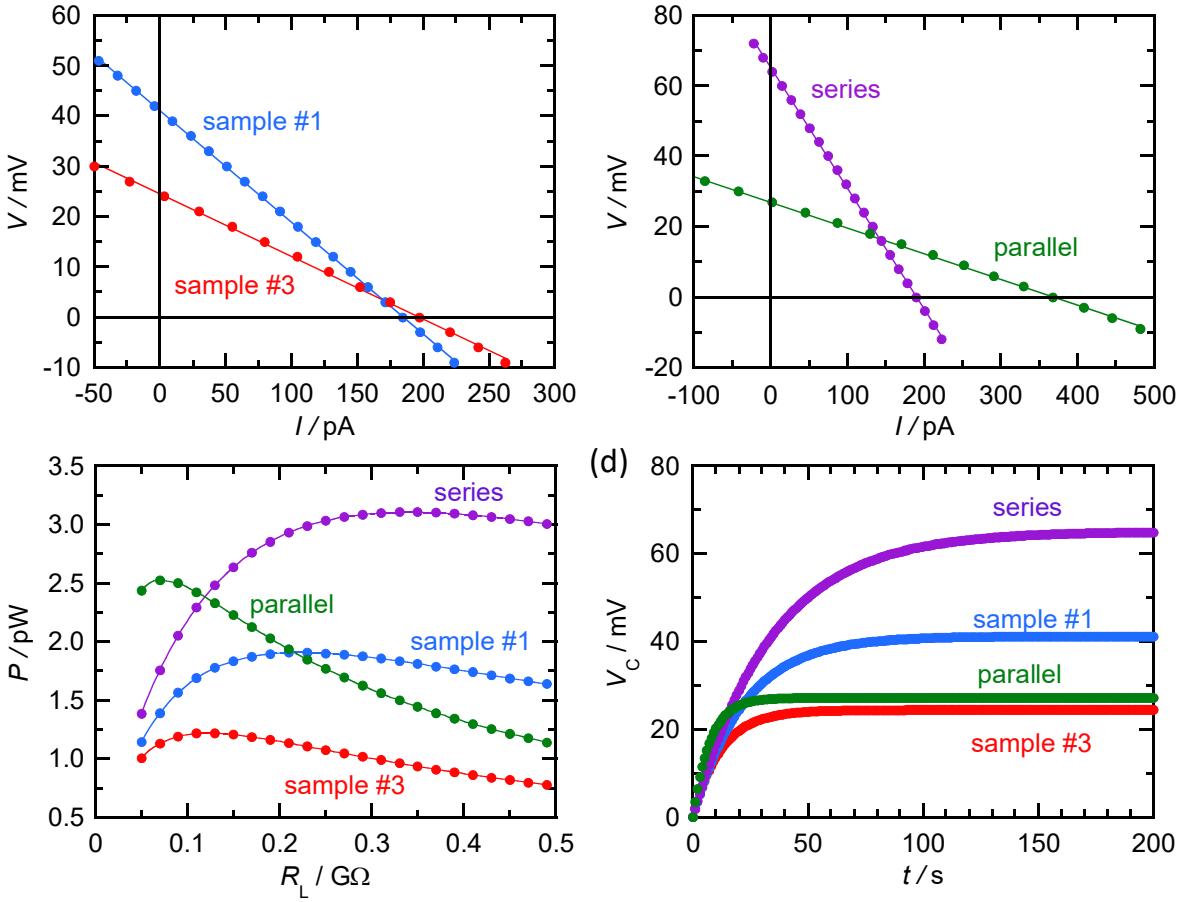

Fig. 7 (a) *V–I* curves and Thévenin equivalent circuits for two nanofluidic cells based on nanopore *samples #1* and *#3*. We use the experimental methods of Fig. 2 for position 1, with c_L

= 10 mM and c_R = 100 mM KCl. (b) *V–I* curves and Thévenin equivalent circuits for the series and parallel arrangements of the two nanofluidic cells of Fig. 7a. (c) Power dissipated as a function of the load resistance R_L for the two nanofluidic cells and their series and parallel arrangements obtained with the parameters of Figs. 7a and 7b. (d) Charging curves for a capacitor of capacitance C = 0.1 μF obtained for the two nanofluidic cells and the series and parallel arrangements.

	Sample #1	Sample #3	Series, exp	Series, theo	Parallel, exp	Parallel, theo
V_{Th} / mV	41.1	24.5	65.2	65.6	27.0	30.5
R_{Th} / GΩ	0.222	0.125	0.343	0.347	0.073	0.080
I_N / pA	185	197	190	190	369	382

Table 2. The equivalent circuit characteristics of the nanofluidic cells based on nanopore *samples #1* and *#3* together with those for the series and parallel associations. For the latter case, both experimental and theoretical values are included. Note the validity of the Thévenin voltages and resistances additivity and the Millman's theorem. The cell and circuit experimental conditions are those of Fig. 7. The results for the series additivity are obtained as $V_{Th} = \sum_{i=1}^{N} V_{Th,i}$ and $R_{Th} = \sum_{i=1}^{N} R_{Th,i}$. The results for the parallel arrangement (Millman's theorem) are obtained as $V_{Th} = \left(\sum_{i=1}^{N} \frac{V_{Th,i}}{R_{Th,i}}\right) \Big/ \left(\sum_{i=1}^{N} \frac{1}{R_{Th,i}}\right)$ and $\frac{1}{R_{Th}} = \sum_{i=1}^{N} \frac{1}{R_{Th,i}}$.

For the sake of future applications, Figs. 8a–d consider the scaling of the single pore results to the multipore case. The membrane *sample #4* contains 300 pores approximately. Fig. 8a shows the voltage V_{Th} as a function of the concentration c_R can now be compared with Fig. 4a. Fig. 8b gives the power dissipated in the load resistor as a function of R_L for c_L = 10 mM

and c_R = 100 mM KCl. The differences observed between theory and experiments should be ascribed to the absence of a trivial direct proportionality between the single pore and multipore case because of the effect of the diffusion boundary layers flanking the membrane [16]. Fig. 8c shows the time dependence of the circuit current because of the changes occurring in in the nanofluidic cell when it is connected to the external resistor R_L. After an operation time of 4 h, the current decreased to 60 % approximately. Fig. 8d gives the Thévenin equivalent initially (zero time) and after 4 h of operation times. The decrease of Thévenin equivalent voltage and resistance can be ascribed to the leakage processes in the salt bridges of the electrodes after a long operation time.

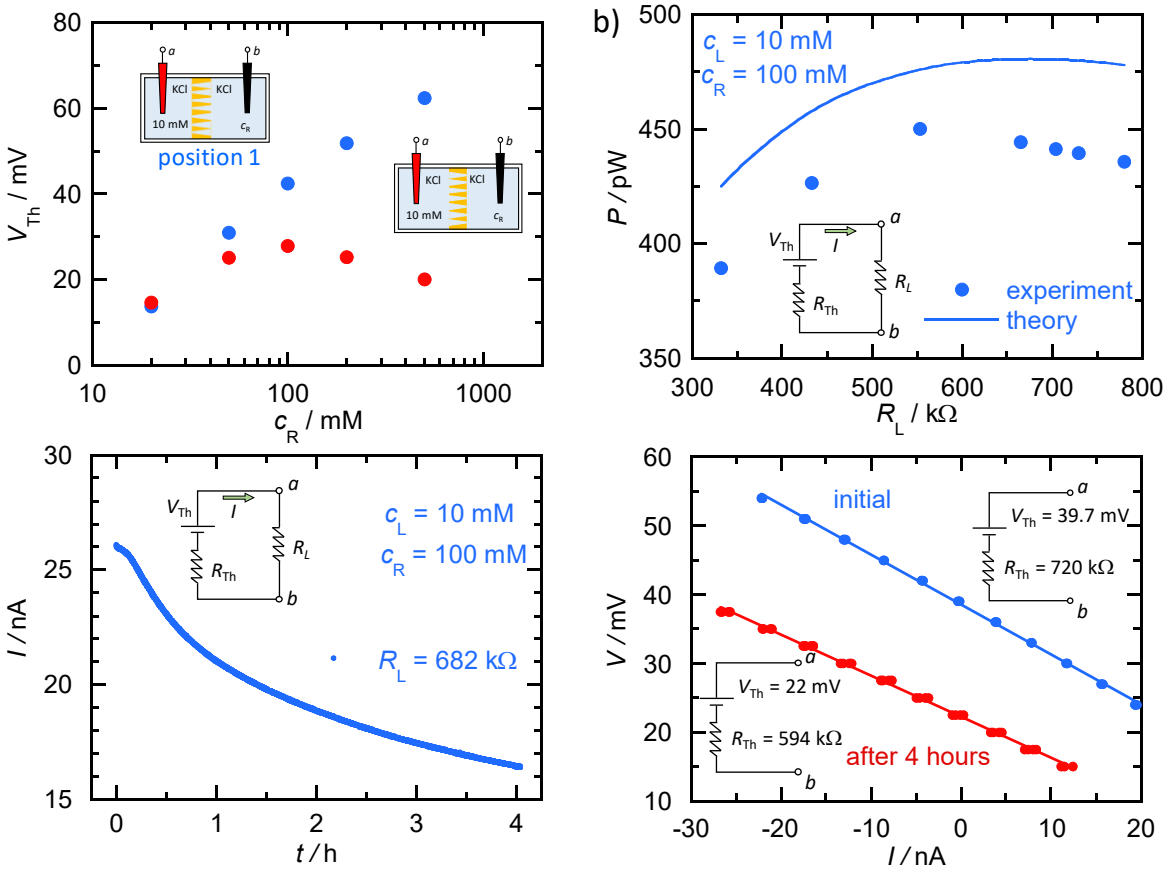

Fig. 8 (a) The voltage V_{Th} as a function of the concentration c_R for multipore *sample #4*. (b) The power dissipated in the load resistor (*inset*) as a function of R_L for c_L = 10 mM and c_R = 100 mM KCl. (c) The time dependence of the circuit current when the nanofluidic cell is connected

to the external resistor R_L (*inset*). (d) The Thévenin equivalent circuits (*insets*) initially and after 4 h of operation times.

4. Conclusion

Single-nanopore membranes and nanofluidic concentration cells are central to electrochemical devices [4,6–10]. The electrical coupling of ionic conduction to electronic components such as load capacitors and resistors provides functionality to the resulting hybrid circuits. We have analyzed the validity of basic principles governing electric circuit theory such as the Thévenin equivalent circuit, the voltages and resistances additivity, and the Millman theorem in nanofluidic cells. To this end, we have considered a wide range of experimental conditions concerning salt concentrations, nanostructure asymmetry, electrical capacitance, series and parallel arrangements, and number of membrane pores from an applied electrochemistry perspective that should be useful to nanofluidics. The results obtained suggest that basic circuit models provide approximate tools to guide the analysis and characterization of electrochemical concentration cells.

CRediT authorship contribution statement

Patricio Ramirez: Conceptualization, Investigation, Methodology, Formal analysis, Writing – review & editing. **Javier Cervera:** Formal analysis, Supervision, Project administration, Funding acquisition. **Vladimir García-Morales:** Investigation, Formal analysis, Writing – review & editing. **Saima Nasir:** Investigation, Methodology, Formal analysis. **Mubarak Ali:** Investigation, Methodology, Formal analysis, Writing – review & editing. **Wolfgang Ensinger:** Supervision, Project administration, Funding acquisition. **Salvador Mafe:** Conceptualization, Methodology, Formal analysis, Writing – original draft.

Declaration of Competing Interest

The authors declare that they have no known competing financial interests or personal relationships that could have appeared to influence the work reported in this paper.

Data availability

Data will be made available on request.

Acknowledgments

P.R., J.C., V.G., and S.M. acknowledge the support from the *Ministerio de Ciencia, Innovación y Universidades* (Spain) and the *European Regional Development Funds* (FEDER), project No. PID2022-139953NB-I00. M.A., S.N, and W.E. acknowledge the funding from the Hessen State Ministry of Higher Education, Research and the Arts, Germany, under the LOEWE project iNAPO.

References

[1] Z. S. Siwy, M.L. Bruening, S. Howorka, Nanopores: synergy from DNA sequencing to industrial filtration – small holes with big impact, Chem. Soc. Rev. 52 (2023)1983 – 1994. https://doi.org/10.1039/D2CS00894G.

[2] J. Cervera, M. Levin, S. Mafe, Bioelectricity of non-excitable cells and multicellular pattern memories: Biophysical modeling, Phys. Rep. 1004 (2023) 1 – 31. https://doi.org/10.1016/j.physrep.2022.12.003.

[3] Y. Hou, Y. Ling, Y. Wang, M. Wang, Y. Chen, X. Li, X. Hou, Learning from the brain: bioinspired nanofluidics, J. Phys. Chem. Lett. 14 (2023) 2891 – 2900. https://doi.org/10.1021/acs.jpclett.2c03930.

[4] P. Ramirez, V. Gomez, J. Cervera, S. Nasir, M. Ali, W. Ensinger, S. Mafe, Energy conversion from external fluctuating signals based on asymmetric nanopores, Nano Energy 16 (2015) 375 – 382. https://doi.org/10.1016/j.nanoen.2015.07.013.

[5] M. Tagliazucchi and I. Szleifer, Transport mechanisms in nanopores and nanochannels: can we mimic nature?, Mater. Today 18 (2015) 131 – 142. https://doi.org/10.1016/j.mattod.2014.10.020.

[6] K. Xiao, L. Wen, L. Jiang, Biomimetic solid-state nanochannels: From fundamental research to practical applications, Small 12 (2016) 2810 – 2831. https://doi.org/10.1002/smll.201600359.

[7] C. Verdia-Baguena, V. Gomez, J. Cervera, P. Ramirez, S. Mafe, Energy transduction and signal averaging of fluctuating electric fields by a single protein ion channel, Phys. Chem. Chem. Phys. 19 (2017) 292 – 296. https://doi.org/10.1039/C6CP06035H.

[8] V. Gomez, P. Ramirez, J. Cervera, M. Ali, S. Nasir, W. Ensinger, S. Mafe, Concatenated logic functions using nanofluidic diodes with all-electrical inputs and outputs. Electrochem. Commun. 88 (2018) 52 – 56. https://doi.org/10.1016/j.elecom.2018.01.016.

[9] G. Perez-Mitta, A.G. Albesa, C. Trautmann, M.E. Toimil-Molares, O. Azzaroni, Bioinspired integrated nanosystems based on solid-state nanopores: "iontronic" transduction of biological, chemical and physical stimuli, Chem. Sci. 8 (2017) 890 – 913. https://doi.org/10.1039/C6SC04255D.

[10] T. Ma, J.-M. Janot, S. Balme, Track-etched nanopore/membrane: from fundamental to applications, Small Methods 4 (2020) 2000366. https://doi.org/10.1002/smtd.202000366.

[11] E. Sempou, V. Kostiuk, J. Zhu, C.M. Guerra, L. Tyan, W. Hwang, E. Camacho-Aguilar, M.J. Caplan, D. Zenisek, A. Warmflash, N.D.L. Owens, M.K. Khokha, Membrane potential drives the exit from pluripotency and cell fate commitment via calcium and mTOR., Nat. Commun. 13 (2022) 6681. https://doi.org/10.1038/s41467-022-34363-w.

[12] P. Ramirez, J. Cervera, V. Gomez, M. Ali, S. Nasir, W. Ensinger, S. Mafe, Membrane potential of single asymmetric nanopores: Divalent cations and salt mixtures, J. Membrane Sci. 573 (2019) 579 – 587. https://doi.org/10.1016/j.memsci.2018.12.043.

[13] J. Gao, X. Liu, Y. Jiang, L. Ding, L. Jiang, W. Guo, Understanding the giant gap between single-pore- and membrane-based nanofluidic osmotic power generators, Small 15 (2019)1804279. https://doi.org/10.1002/smll.201804279.

[14] S. Balme, T. Ma, E. Balanzat, J.-M. Janot, Large osmotic energy harvesting from functionalized conical nanopore suitable for membrane applications, J. Membrane Sci. 544 (2017) 18 – 24. https://doi.org/10.1016/j.memsci.2017.09.008.

[15] G. Laucirica, A. G. Albesa, M. E. Toimil-Molares, C. Trautmann, W. A. Marmisolle, O. Azzaroni, Shape matters: Enhanced osmotic energy harvesting in bullet-shaped nanochannels, Nano Energy 71 (2020) 104612. https://doi.org/10.1016/j.nanoen.2020.104612.

[16] L. Wang, Z. Wang, S. K. Patel, S. Lin, M. Elimelech, Nanopore-based power generation from salinity gradient: Why it is not viable, ACS Nano 15 (2021) 4093 – 4107. https://doi.org/10.1021/acsnano.0c08628.

[17] M.H. Ali Haider, S. Nasir, M. Ali, P. Ramirez, J. Cervera, S. Mafe, W. Ensinger, Osmotic energy harvesting with soft-etched nanoporous polyimide membranes, Mater. Today Energy 23 (2022) 100909. https://doi.org/10.1016/j.mtener.2021.100909.

[18] P. Ramirez, V. Garcia-Morales, V. Gomez, M. Ali, S. Nasir, W. Ensinger, S. Mafe, Hybrid circuits with nanofluidic diodes and load capacitors, Phys. Rev. Applied 7 (2017) 064035. https://doi.org/10.1103/PhysRevApplied.7.064035.

[19] M. Ali, P. Ramirez, S. Nasir, J. Cervera, S. Mafe, W. Ensinger, Ionic circuitry with nanofluidic diodes, Soft Matter 15 (2019) 9682 – 9689. https://doi.org/10.1039/C9SM01654F.

[20] P. Apel, Track etching technique in membrane technology, Radiat. Meas. 34 (2001) 559 – 566. https://doi.org/10.1016/S1350-4487(01)00228-1.

[21] Z. Siwy, D. Dobrev, R. Neumann, C. Trautmann, K. Voss, Electro-responsive asymmetric nanopores in polyimide with stable ion-current signal, Appl. Phys. A 76 (2003) 781 – 785. https://doi.org/10.1007/s00339-002-1982-7.

[22] P. Apel, V. Bashevoy, I.V. Blonskaya, N.E. Lizuno, Shedding light on the mechanism of asymmetric track etching: an interplay between latent track structure, etchant diffusion and osmotic flow, Phys. Chem. Chem. Phys. 18 (2016) 25421 – 25433. https://doi.org/10.1039/C6CP05465J.

[23] Y. Green, Y. Edri, G. Yossifon, Asymmetry-induced electric current rectification in permselective systems, Phys. Rev. E 92 (2015) 033018. https://doi.org/10.1103/PhysRevE.92.033018.

[24] P. Ramírez, P.Y. Apel, J. Cervera, S. Mafe, Pore structure and function of synthetic nanopores with fixed charges: tip shape and rectification properties, Nanotechnology 19 (2008) 315707. https://doi.org/10.1088/0957-4484/19/31/315707.

[25] P.B. Peters, R. Van Roij, M.Z. Bazant, P.M. Biesheuvel, Analysis of electrolyte transport through charged nanopores, Phys. Rev. E 93 (2016) 053108. https://doi.org/10.1103/PhysRevE.93.053108.

TOC Entry